International Journal on Interactive Design and Manufacturing (IJIDeM) (2024) 18:1183–1193
https://doi.org/10.1007/s12008-023-01732-8

ORIGINAL ARTICLE

Fatigue life of super duplex stainless steel sheets (UNS S32750) as influenced by micro plasma arc welding parameters: an investigation using the surface response method

Sasidhar Gurugubelli[1] · **V. V.S. Kesava Rao**[2]

Received: 27 September 2023 / Accepted: 15 December 2023 / Published online: 12 January 2024

Abstract
Duplex steels play a vital role in manufacturing pipeline and ducts where they are exposed to severe corrosion environment. The inquiry into the optimal conditions for Micro Plasma Arc Welding (MPAW) has not yielded any definitive results, despite its intrinsic application for joining thin sheets in manufacturing industries, particularly in aerospace and automobile parts. (SDSS) Super duplex stainless steel UNS S32750 of 0.33 mm thin Sheet is butt welded utilizing MPAW in this work. The fatigue qualities must be studied due to frequent loading in service. Peak current, base current, pulse rate and pulse width are significant welding input parameters and fatigue life is the output. High cycle fatigue testing is done in tension-tension mode in this work. Keeping stress ratio at 0.1, loading is applied sinusoidally between 0.6 kN and 6 kN. Response Surface Method (RSM) amid Central Composite Design (CCD) is used to conduct 31 different experimental permutations, while keeping in mind four variables and five weld input parameter levels. Weld input parameters are varied, and the resulting charts show how the output responses change. Minitab software is used to create linear function-based mathematical models. At a confidence level of 95%, Analysis of Variance (ANOVA) is conducted. Surface Response Optimizer is used to calculate optimal fatigue life.

Keywords Micro plasma Arc Welding · Fatigue life · UNS S32750 SDSS · Response surface method (RSM)

1 Introduction

Due to their high strength and low Ni content, SDSS has considerable intensive advantage over different SS. When chloride attack is a major concern, design engineers often choose DSS over austenitic stainless steels for enclosing and constructing assemblies because of the material's great resistance to pitting corrosion. Maintaining a microstructure with a minimal number of secondary phases, for instance austenite (γ) and delta-ferrite (δ), is what gives DSS its beneficial properties. The ideal microstructure of DSS could be damaged by any thermal treatment above 300ºC, including fusion welding [1–3]. Weld metal composition and cooling rate are significant factors in determining the composition of the DSS metal after welding. It is ferrite that is more stable at higher cooling speeds and aid in increasing the likelihood of nitride precipitation, but these effects are highly dependent on heat input, pre-heating, and inter-pass temperatures throughout welding operations [4, 5]. Welding times are lengthened due to the slow cooling rates which raise the prospect of spinodal breakdown of Cr-rich-ferrite (α1), apparently 475ºC precipitation and weakening of intermetallic, include Sigma (σ) and Chi (χ) [6]. Thus, in order to attain moderate cooling rates, conventional multi-pass fusion welding requires heat input to be within strict upper and lower limits and inter-pass temperatures to be kept reasonably low (180-200ºC) [1, 7]. Additional time and effort are required in typical multi-pass welding methods for controlling such low-tolerance welding parameters.

If the solidified microstructure can be managed, single-pass welding of DSS would allow for greater welding

✉ Sasidhar Gurugubelli
sasidhar.g@gmrit.edu.in

[1] Mechanical Department, Andhra University, Faculty of Mechanical Deparment, GMR Institute of Technology, Rajam, India

[2] Mechanical Department, Andhra University, Visakhapatnam 530003, India

efficiency and uniformity in metallurgical and mechanical quality. Laser beam welding, Plasma arc welding (PAW), hybrid Laser arc welding and electron beam welding keyhole style can be accustomed to create single-pass weldments of DSS. Since These welding procedures can only be used on connections with a negligible or non-existent gap, it is impossible to incorporate an adequate quantity of filler metal (comprised of too much Ni) into the weld metal to ensure that the resulting alloy has a sufficient amount of γ in δ matrix. Autogenous or partly-autogenous keyhole welding, despite its modest heat inputs [8, 9], can cause an excess of ferrite to develop in the DSS welds, corrosion and toughness are both compromised as a result of this [10, 11]. To get a weld metal microstructure with the right phase balance and no secondary phases, post-weld procedures like solutionizing are typically necessary after PAW, LBW, HLAW, and EBW of DSS [12]. I.Alvarez-Armas et al. [13]. studied the development of cracking in low and high cycle fatigue tests on a duplex stainless steel that had been embrittled. Microcracks cause the ferrite phase to begin during low-cycle fatigue, and this can happen either along the slip planes with the highest Schmid factor (SF) inside the grains or at the a/a grain boundary. Roman Kolmorgen and Horst Biermann [14] investigated the thermo-mechanical fatigue (TMF) characteristics of duplex stainless steel X2CrNiMoN22-5-3. Primary and secondary hardening are clearly visible in the cyclic stress response curves of the duplex steel, Whereas the former agrees with the cyclic hardening regime of the single-phase austenitic steel, the latter agrees with the ferritic steel.Guocai Chai et al. [15] analyzed in-grain and across-grain/phase boundary crack propagation behaviour. Dislocation slip in the grains is responsible for most crack branching, while phase boundaries are responsible for crack deflection. U. Krupp et al. [16] examined the initiation of fatigue cracks and their interactions with initial microstructural barriers using ultrasonic fatigue testing of miniature specimens in conjunction with (i) in-situ observation, (ii) electron backscatter diffraction, (iii) synchrotron computer tomography, and (iv) high-energy X-ray diffraction. Chin-Hyung Lee et al. [17] established a method for calculating the amount by which steel butt welds undergo relaxation after being subjected to cyclic external loading.

Sung-Wook Kang et al. [18] compared the fatigue strength to the S-N curves provided for a series of butt weld specimens welded in both the horizontal (2G) and vertical (3G) positions. The angular distortion of 2G and 3G specimens, as well as their respective effects on fatigue strength, are studied. U. Krupp et al. [19] studied the development of cracks with ultrasonic fatigue testing, electron microscopy, and synchrotron diffraction. It was discovered that the first microstructural barrier has a crucial role in determining Very High Cycle (VHCF) life. Jinwoo Cho and Chin-Hyung Lee [20] Reduction of residual stress under cyclic loading was studied in a girth welded duplex stainless-steel pipe. It is found that residual tensions in and around the girth weld are greatly reduced even after the first few loading cycles, with the degree of stress relaxation depending on the intensity of the cyclic loading. I. S. Cortes-Cervantes et al. [21] carried out gas metal arc welded (GMAW) on plates of AL6XN stainless steel with a higher austenitic content and involving little electromagnetic interaction. Under continuous stress amplitude and uniaxial load, the fatigue behaviour of the welded joints was assessed. Timo Bjork et al. [22] tested the durability of duplex and super-duplex steels against fatigue using a variety of techniques, including practical tests and theoretical analyses that make use of effective notch stress-based procedures like the 4R approach. Eyasin Arafat et al. [23] The influence of friction stir processing (FSP) on the formation of fatigue cracks in super duplex stainless steel was studied (SDSS) SAF 2507. The resistance to fatigue crack development (FCG) and the fatigue life of FSP specimens are found to be greater than those of the base material. Andrew Sales et al. [24] reported fatigue test results and fracture surface fractography of WAAM-processed SDSS, which demonstrated a substantial anisotropy of fatigue characteristics and fatigue crack initiations arising from interior defects rather than surface faults. Andrew Sales et al. [25] modified the interpass temperatures to enhance the fatigue characteristics of the SDSS produced by WAAM. According to their findings, the interpass temperature can play a pivotal role in ensuring that structural components manufactured using the WAAM process have isotropic mechanical characteristics and long fatigue lives. Janardhan Gorti et al. [26] tested the effect of pre-straining HSLA steel sheets on the tensile and fatigue performance of resistance spot- welded joints. Here, super duplex stainless steel (UNS S32750) of 0.33 mm thick sheets were selected. They are welded together using MPAW. In the present work Fatigue test was carried out at a constant frequency of $10H_z$. One may try at other frequencies based on the thickness of the material. The purpose of this paper is to investigate the relationship between fatigue life and welding parameters.

Table 1 UNS S32750 chemical composition (weight%)

Cr	Ni	Fe	Mo	Mn
25.04	6.69	64.02	3.25	1.00

2 Materials and methodology

UNS S32750 SDSS sheets measuring 240 × 100 × 0.33 milli meters are autogenously joined with a square butt joint. The chemical composition and tensile characteristics of UNS S32750 SDSS are listed in Tables 1 and 2. In an effort to avoid the absorption of atmospheric oxygen and nitrogen

Table 2 UNS S32750 mechanical properties

Ultimate Tensile Strength (Mpa)	Elongation (%)	Vickers Hardness (VHN)
923.160	21.8	259.7

Table 3 Welding setup conditions

Source of Power	Secheron Micro Plasma Arc Machine (Model: PLASMAFIX 50E)
Polarity	Direct Current Electrode Negative (DCEN)
Modus operandi	Pulse
Electrode	2% thoriated tungsten electrode
The Size of the Electrode	1 mm
Plasma-like gas	Hydrogen & Argon
Rate of gaseous plasma flow	6 (Lpm)
Gas shielding	Argon
Rate of flow of shielding gas	0.6 (Lpm)
Gas for purging	Argon
Gas flow rate during purging	0.6 (Lpm)
Diameter of the copper nozzle	1 mm
Distancing of Nozzle from Plate	1 mm
Rate of Welding	240 mm/min
Position of Torch	Vertical
Mode of Procedure	Automatic

Table 4 Welding parameters and bounds

Element	Levels				
	+2	+1	0	-1	-2
Peak Current (Amp)	22	21	20	19	18
Base Current (Amp)	12	11	10	9	8
Pulse rate (Pulses /Second)	60	50	40	30	20
Pulse width (%)	70	60	50	40	30

during and immediately following welding, high purity argon gas (99.99%) is utilized as a shielding gas and as a trailing gas. Welding was carried out using the parameters specified in Table 3. Quality of the weld features of the MPAW process are affected by a wide variety of process parameters, including but not limited to peak current, base current, pulse rate and pulse width.

From the works reported by Sasidhar et al. [27] and Siva Prasad et al. [28] and observed that the peak current, back current, pulse rate and pulse width are the most important factors influencing weld quality. The input parameters are selected based on the works reported by earlier researchers on PAW of thin sheets. The values of the chosen input parameters are arrived based on trial experiments conducted by varying each parameter separately, by keeping other parameters constant. Table 4 displays the selected values for input parameters.

3 Experimentation

Testing for high cycle fatigue is conducted in a tension-tension configuration. Applying a sinusoidal load between 0.6 and 6 kilonewtons while maintaining a stress ratio of 0.1. Experimental setup is shown in Fig. 1a, b; Table 5 displays the results of an analysis of the fatigue life of the weld joints for each of the samples taken. Figure 1c shows wire cut fatigue specimens prepared in accordance with ASTM E647- 04 standards. Each welded sample was processed by electro-discharge machining in the weld transverse direction. Using a 100 KN Fatigue testing machine with computer-controlled servo hydraulic, fatigue tests were conducted (INSTRON, Model No: 8801).

When engineering buildings or components that will be subjected to repeated loading and unloading cycles, it is essential to predict the fatigue life of the materials used. The S-N (stress-life) curve method is one of the most used empirical formulas and conventional approaches to fatigue life estimation. One way to visualize the results of fatigue tests is via the S-N curve, which shows the relationship between the applied stress (S) and the number of cycles until failure (N). A logarithmic scale is usually used to plot the curve. A common way to represent the S-N curve is:

Table 5 displays the experimental results of fatigue tests that were used to derive the constants A and B.

4 Statistical analysis – empirical relationships

Process parameter optimization using response surface methods and empirical relationship establishment were both aided by the design expert software.

4.1 Main effect plot

Main effect plot is drawn for fatigue life at a frequency of 10 Hz as shown in Fig. 2. A higher peak current result in a longer fatigue life. This is because the high current causes a great deal of heat, causing the base metal to properly fuse. Base current extends fatigue life by keeping the peak current steady during pulse welding. Overheating and inadequately fusing the weld joint lead to incorrect fusion of the base metal, reducing its fatigue life. Weld joint strength is reduced because of poor fusing caused by a wider pulse width. Therefore, the pulse width has a negative effect on fatigue strength. In addition, a larger time gap between pulses might cause the weld joint to cool more quickly, leading to coarser grains and a shorter fatigue life.

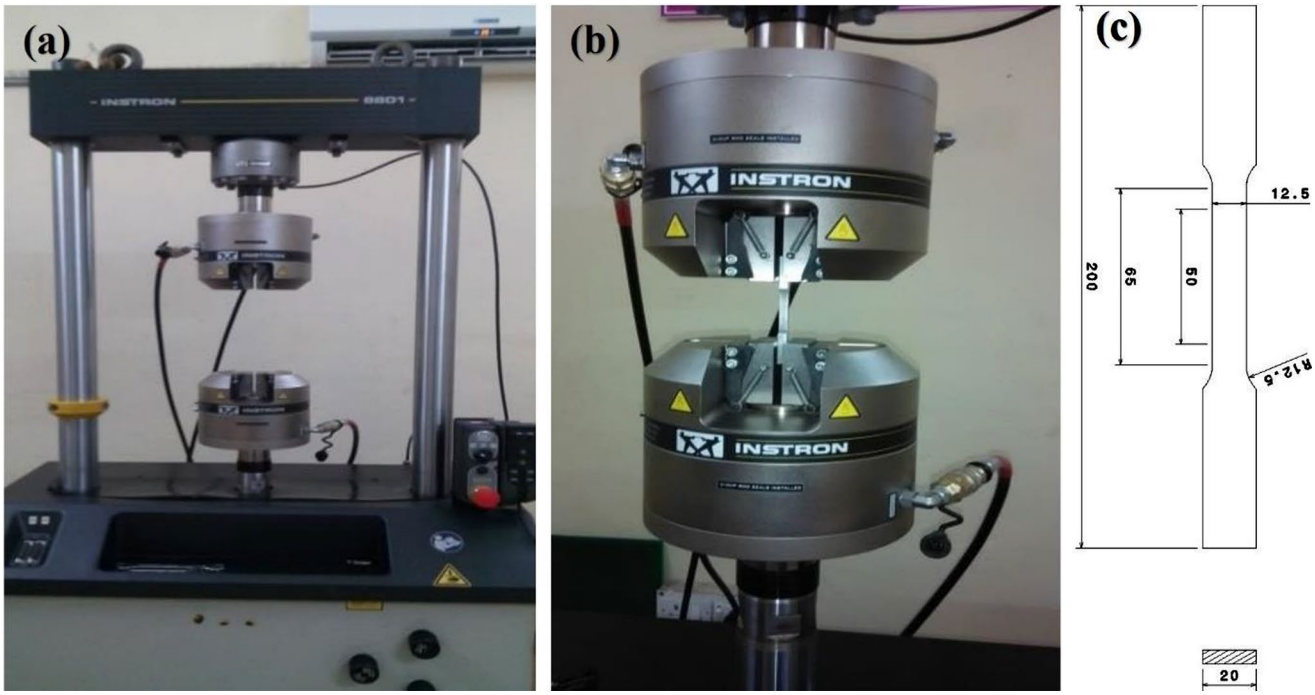

Fig. 1 (**a**) Fatigue testing machine, (**b**) Hydraulic grippers, (**c**) Fatigue specimen as per ASTM E6474-04

4.2 Mathematical modelling

In RSM, a number of statistical and numerical methods are used to determine the optimal response based on the given range of values for the dependent and independent variables. Response Y from the response surface model is provided as the solution of a second-order polynomial equation with four factors, as shown in Eq. 1.

$$Y = b_o + \sum b_i X_i + \sum b_{ij} X_i^2 + \sum \sum b_{ij} X_i X_j + \in \tag{1}$$

In the equation, the output function Y stands in for the set of parameters x_i to x_j. where b_o, b_i and b_j are the coefficients of the polynomial and $\in$ represents noise. The current research uses RSM for optimization purposes in order to increase fatigue life. The fatigue life is the output that can be optimized in MPAW, and it is a function of the peak current (I_p), base current (I_b), pulse rate (G), and pulse width (D). Equation 2 provides a mathematical connection to the aforementioned statement:

$$\text{Fatigue life, } F_L = f\left(I_p,\ I_b,\ G,\ D\right) \tag{2}$$

The empirical relation is constructed using MINTAB software to predict the response is given below in Eq. (3):

$$\begin{aligned} F_L = {} & 249922.7 + 1911.2\,(I_p) \\ & + 1452\,(I_b) - 973.5\,(G) \\ & - 211.7\,(D) + 679.2\,(Ip)^2 \\ & + 165.3\,(G)^2 - 2605\,(I_p \times G) \\ & + 559.5\,(I_p \times D) + 10.543\,(I_b \times G) \\ & - 12.155\,(I_b \times D) \end{aligned} \tag{3}$$

4.3 Analysis of variance (ANOVA)

Statistical analysis of variance (ANOVA) is used to measure the precision of the models. Based on this method, a value is considered to be acceptable at the confidence limit if its estimated F_{ratio} value is lesser than the standard F_{ratio} value (F-table value 2.56) at 95% confidence level. Table 6 displays the outcomes of an analysis of variance performed on Fatigue Life. Based on the results in Table 6, it can be seen that the computational models produced are satisfactory at the 95% confidence level. Coefficient of determination 'R^2' for the above developed models is determined to be around 0.98. P values under 0.05 indicate that the model term is statistically significant. The relationship between experimental factors and responses is strongly indicated by a lack-of-fit.

The scatter plot is generated to see the difference between the expected and experimental values. Predicted values are computed by substituting the weld input parameters in the empirical mathematical equation developed by considering only the significant coefficients. If the experimental and

Table 5 Experimental and predicted responses

Input elements					Experimental	Predicted
Exp. No.	Peak Current, Ip (Amps)	Base Current, Ib (Amps)	Pulse Rate, G (Pulses/Sec)	Pulse Width, D (%)	Fatigue Life (cycles)	Fatigue Life (cycles)
1	19	9	30	40	19965.4	18944.9
2	21	9	30	40	27,177	27279.7
3	19	11	30	40	22584.8	22981.5
4	21	11	30	40	29622.4	30475.7
5	19	9	50	40	22,238	23190.3
6	21	9	50	40	20888.3	21102.9
7	19	11	50	40	36579.8	36,545
8	21	11	50	40	33170.7	33616.8
9	19	9	30	60	28431.3	28413.9
10	21	9	30	60	22750.9	24986.8
11	19	11	30	60	21580.7	21708.2
12	21	11	30	60	31,964	31440.4
13	19	9	50	60	21889.9	21378.7
14	21	9	50	60	21497.2	21529.2
15	19	11	50	60	23,665	23,991
16	21	11	50	60	21938.3	23300.9
17	18	10	40	50	23,541	23817.1
18	22	10	40	50	32508.8	31461.9
19	20	8	40	50	23067.1	23387.8
20	20	12	40	50	30287.6	29196.1
21	**22**	**12**	**20**	**30**	**35787.27**	**38040.1**
22	20	10	60	50	25493.5	24485.1
23	20	10	40	30	26851.1	26281.4
24	20	10	40	70	25635.5	25434.5
25	20	10	40	50	24205.8	24922.7
26	20	10	40	50	24,304	24922.7
27	20	10	40	50	24,620	24922.7
28	20	10	40	50	25,280	24922.7
29	20	10	40	50	25,304	24922.7
30	20	10	40	50	24,605	24922.7
31	20	10	40	50	26,140	24922.7

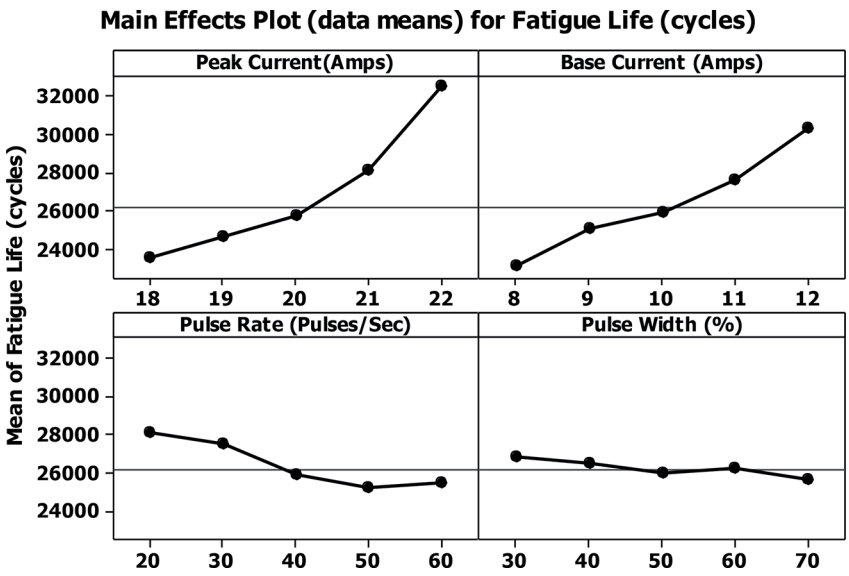

Fig. 2 Main effects on fatigue life

Table 6 Fatigue life (cycles) values using ANOVA

Origin	DoF	Seq SS	Adj SS	Adj MS	F	P
Regression	14	623,843,695	623,843,695	44,560,264	57.05	0.000
Linear	4	162,088,362	162,088,362	40,522,090	51.88	0.000
Square	4	17,938,803	17,938,803	4,484,701	5.74	0.005
Interaction	6	443,816,530	443,816,530	73,969,422	94.70	0.000
Residual Error	16	12,497,934	12,497,934	781,121		
Lack-of-Fit	10	9,653,765	9,653,765	965,377	2.04	0.199
Pure Error	6	2,844,168	2,844,168	474,028		
Total	30	636,341,628				

where SS = Sum of Squares, DoF = Degree of Freedom, MS = Mean Square, F = Fisher's Ratio

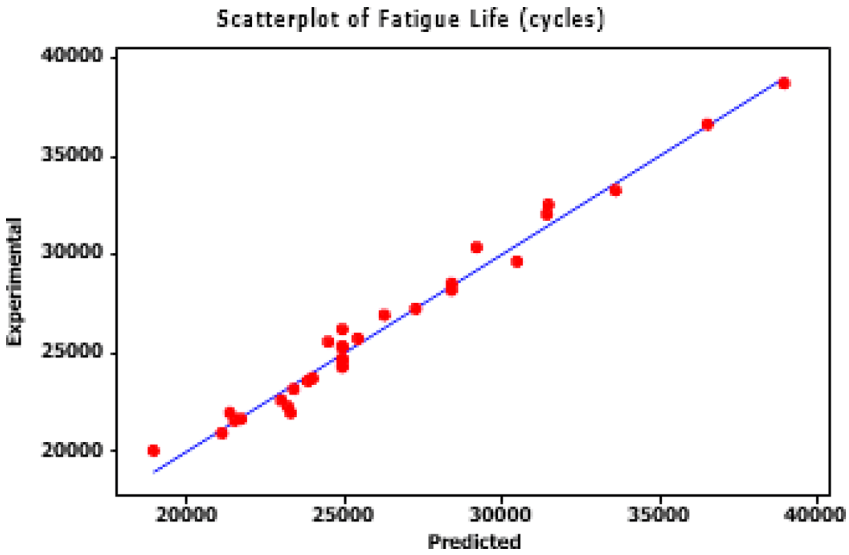

Fig. 3 Predicted values versus experimental values of fatigue life

predicted values are same, then we obtain a proportionality curve from the centre of the axis. However due to error present in the developed empirical model, the experimental and predicted values will vary slightly from proportionality curve. If error can be positive or negative. Hence, we can scatter points on the curve. The high appropriateness of the model is demonstrated by the small scatter between the anticipated and observed values. The results are scatter at 10% deviation. The average value is reported in Fig. 3.

4.4 Optimization of process parameters: contour plots

The fatigue life of weld joint contours, as illustrated in Fig. 4(a) to 4(f), provides valuable insights into the influence of welding parameters. Contour graphs are essential in this analysis, helping to determine the most influential welding parameters on fatigue life. Each figure represents a different set of parameters, and the contours visually represent how these parameters affect the output. Circular contours suggest that both parameters exert an identical level of control on the output, indicating a balanced influence. Conversely, elliptical contours reveal an asymmetry in influence, with the parameter closer to the primary axis having a more significant impact on the output response. When contours are elliptical, one parameter is more dominant in shaping the fatigue life. The elongation of the ellipse along a particular axis indicates the direction of higher influence. This information aids in understanding the sensitivity of the fatigue life to different welding parameters. In cases where contours diverge, the impact on the output response is minimal. Diverging contours suggest that changes in these parameters within the analyzed range have a limited effect on the fatigue life. This insight is crucial for optimizing welding processes, as it helps identify the parameters that require more precise control to enhance fatigue life.

4.5 Optimization of process parameters: surface plots

In the pursuit of optimizing welding parameters for the fatigue life of a weld joint, the analysis involves plotting surfaces and assessing their curvature. Figure 5(a) to 5(f) display surface plots representing the fatigue life of the weld joint under different parameter combinations. These plots are instrumental in identifying optimal values that

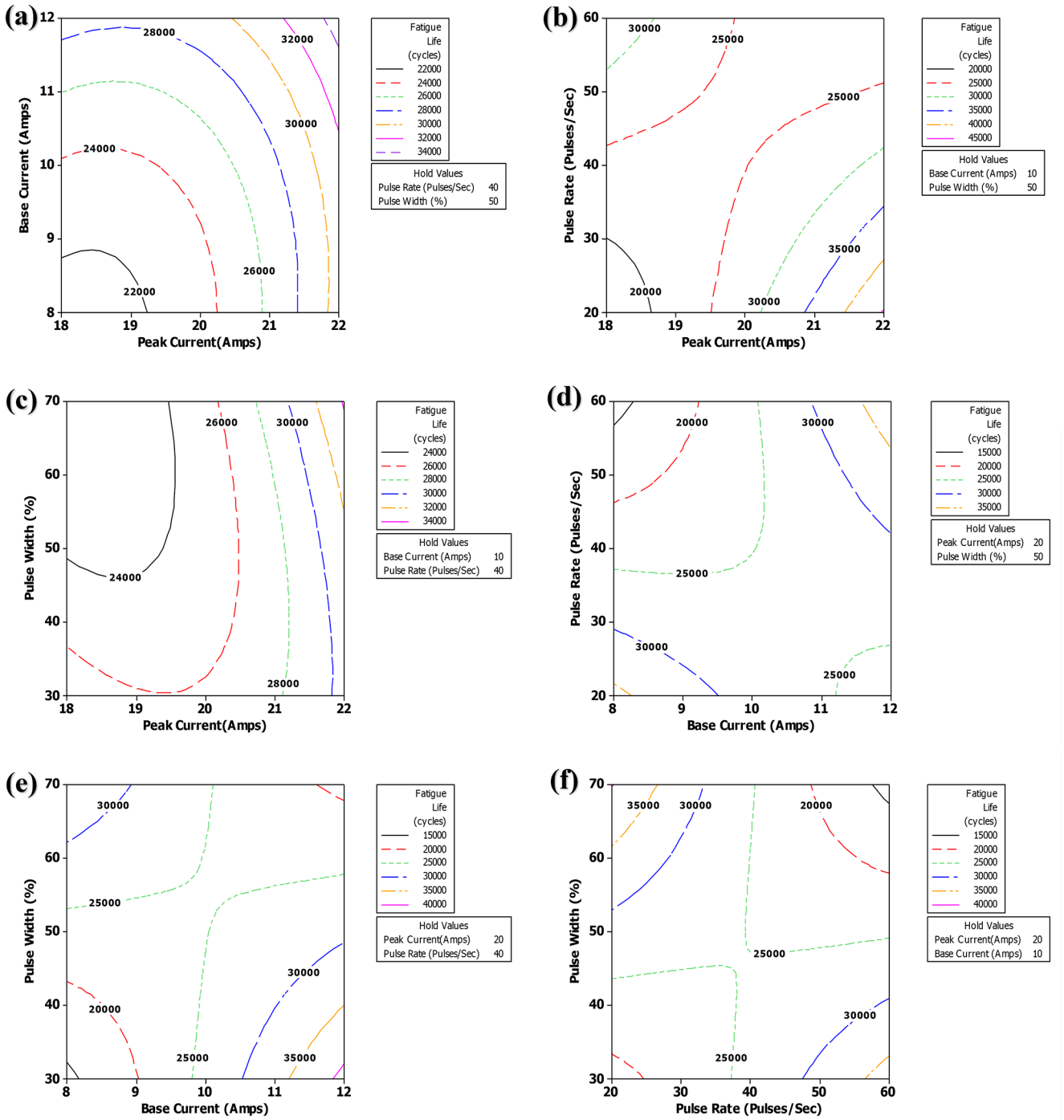

Fig. 4 Fatigue life responses and contours (**a**) Comparison of peak and base current, (**b**) Peak current vs. pulse rate, (**c**) Pulse width vs. peak current (**d**) Pulse rate against base current, (**e**) Base current versus pulse width and (**f**) Rate of pulse versus pulse width

contribute to prolonged fatigue life. The surfaces' curvature is a key factor in this analysis. The apex of the curve surface denotes the highest value, representing the most favorable condition for fatigue life. Conversely, the nadir of the curve surface signifies the least value, representing conditions leading to the shortest fatigue life. Understanding the curvature of these surfaces aids in pinpointing the critical points that significantly influence the weld joint's fatigue performance. The primary goal in this context is to extend the time until a weld joint experiences fatigue failure. Surface plots act as visual aids, approximating the relationship between two variables and revealing trends that impact fatigue life. By examining the surfaces, researchers and engineers can identify trends, patterns, and relationships

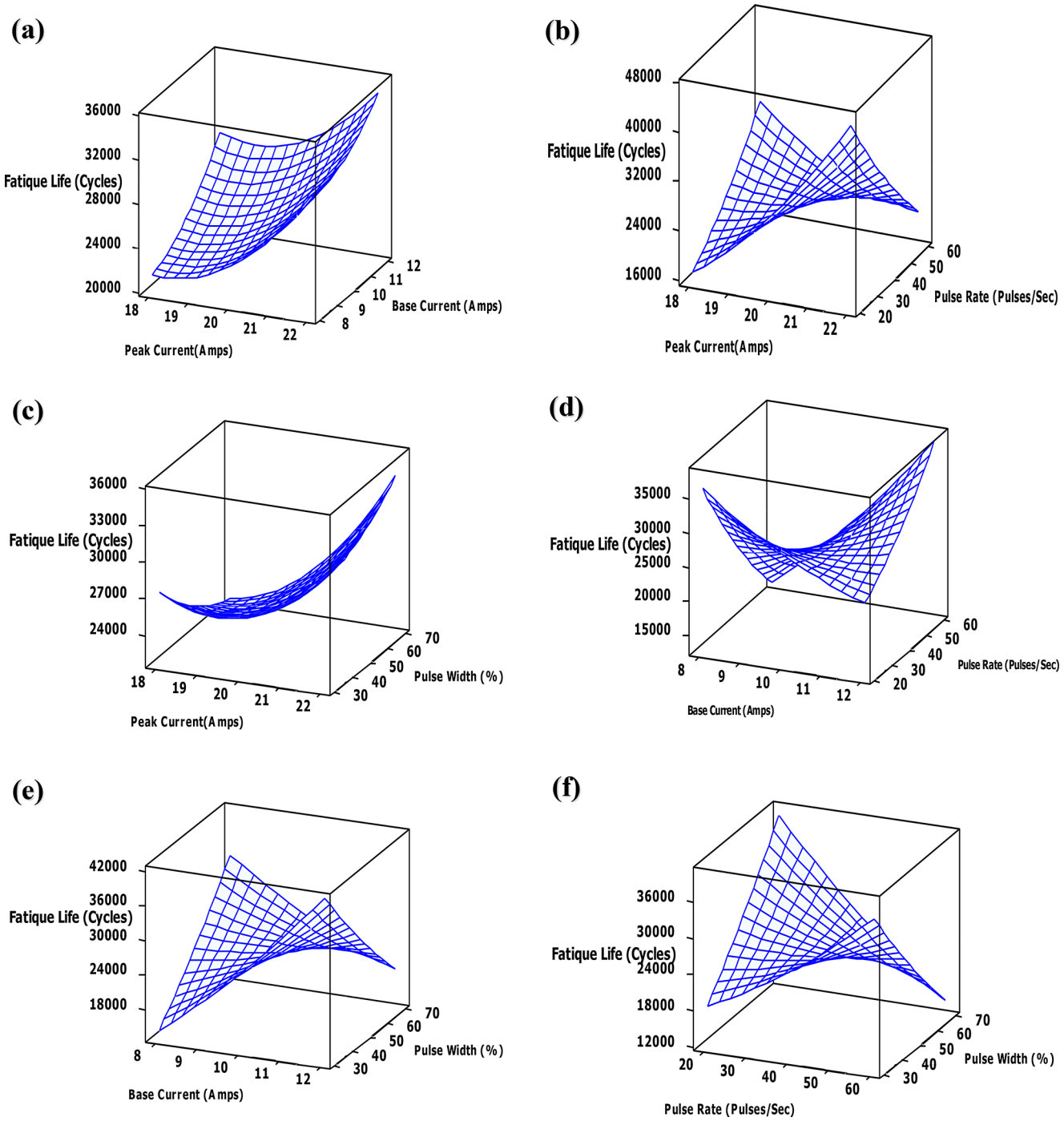

Fig. 5 Fatigue life surface plot responses (**a**) Comparison of peak and base current, (**b**) Peak current vs. pulse rate, (**c**) Pulse width vs. peak current (**d**) Pulse rate against base current, (**e**) Base current versus pulse width and (**f**) Rate of pulse versus pulse width

that contribute to the fatigue behavior of the weld joint. The MINITAB surface response optimizer is employed to determine the ideal combination of welding parameters. This tool uses statistical algorithms to navigate the surface plots and identify the optimal set of parameter values that maximize fatigue life. The optimizer streamlines the process of finding the optimal combination, enabling efficient and effective decision-making in welding parameter selection.

Maximum fatigue life is attained at a I_p of 22 Amps and a I_b of 12 Amps, as shown in Fig. 5 (a). It can be shown in Fig. 5 (b) that a I_p of 22 Amps and a pulse rate of 20 pulses/sec yield the longest fatigue life. Maximum fatigue life was achieved at I_p of 22 Amps and pulse width of 70%,

Table 7 Optimal solution set from RSM

I_p (Amps)	I_b (Amps)	G (Pulses/Sec)	D (%)	Fatigue Life (cycles) (Experimental)	Fatigue Life (cycles) (Predicted)
22	12	20	30	35787.27	38,040

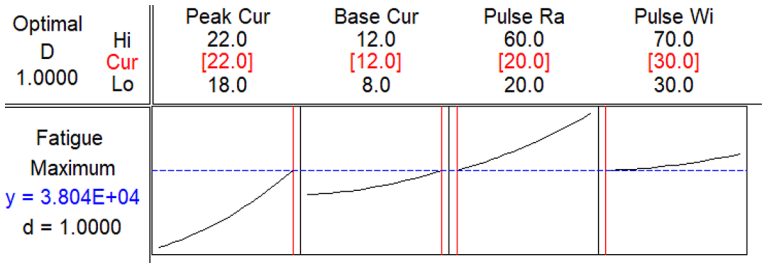

Fig. 6 Optimal values for fatigue life response

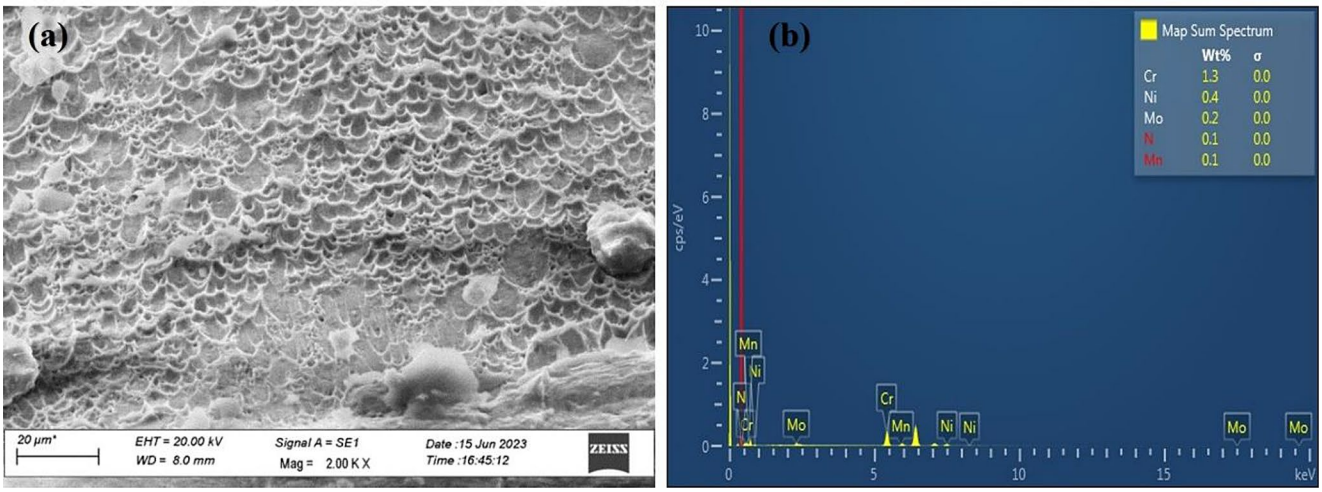

Fig. 7 (**a**) SEM picture shows dimples at the failure zone, (**b**) EDS element analysis data

as shown in Fig. 5 (c). Maximum fatigue life, as shown in Fig. 5 (d), is achieved with a I_b of 12 Amps and a pulse rate of 60 pulses/sec. Figure 5 (e) shows that the optimal conditions for maximizing fatigue life are a I_b of 12 Amps and a pulse width of 60%. Maximum fatigue life was achieved at a pulse rate of 20 pulses/sec and a pulse width of 70%, as shown in fig 0.5 (f).

The optimal set of solution was selected for the following conditions as shown in Table 7; Fig. 6. The set shows the best possible Fatigue life achieved using the Response Surface technique. Fatigue Life of 38,040 is achieved at 22 A peak current, 12 A base current, 20 Pulses/Second pulse rate, and a pulse width of 30%.

5 Metallurgical features of optimized joint

Scanning electron microscopy (SEM) pictures are taken to investigate fatigue specimen failure. Dimples at the failure zone, as seen in Fig. 7a, is indicative of ductile fracture. Because austenite is still the predominant phase in both the weld and the base metal, ductile failure is expected. The soft austenitic phase causes significant plastic deformation at the joints. Micro voids and greater volume fractions on dimples can be visible in some spots on the weld zone fractography image. Weld penetration is affected by the peak current. Inadequate peak current range results in insufficient penetration, while exceeding the current limit negatively impacts weld quality through material loss. Geometrical properties of the weld are affected by the flow rate of the pulses and the pulse width. It is possible to dilute the weld metal more effectively through a rise in pulse rate, which is related to the plasma jet.

Figure 7b presents the results of element analysis and the distribution of weldment phases. The analysis reveals valuable insights into the behavior of chromium in the weldment and its impact on phase formation. Chromium has a natural tendency to form carbides, but this tendency is alleviated by its dispersion in the fusion zone. This dispersion leads to the formation of ferrite phases, which are crucial for the mechanical properties of the welded structure. One notable effect observed in the weld is the acceleration of constitutional supercooling due to nitrogen (N). This phenomenon gives rise to equiaxed dendrites in the weld. Equiaxed

dendrites are formed when the rate of constitutional supercooling is increased, resulting in a distinct microstructure in the weld zone. The data further indicate that chromium carbide precipitation is inhibited by the presence of nitrogen, as demonstrated by the analysis [29, 30]. This inhibition is significant for the overall integrity of the weld, as chromium carbide precipitation can lead to detrimental effects on the material's properties. Examining the results of Energy Dispersive X-ray Spectroscopy (EDS) analysis, it is evident that the weldment contains lower levels of chromium (Cr) at 1.3% and nickel (Ni) at 0.4% compared to the base metal. The variations in the concentrations of these elements can be attributed to the welding process, which induces the development of oxides followed by depletion. The welding-induced oxides contribute to the altered composition of the weldment compared to the base metal.

6 Conclusions

The following findings are derived from the experiments.

- UNS S32750 SDSS sheets is butt welded using MPAW at various permutations according to the Taguchi Design Matrix, and observed that fatigue life increases with increase in frequency.
- Fatigue life increases with peak current and base current. This is due to High temperatures cause the metal to expand, forming larger beads on both sides of the base metal.
- There is no much effect of pulse width and pulse rate on fatigue life of the welded sheet. Nevertheless, fatigue life may decrease with raise in pulse width, due to large time interval between the pulses, leading to faster cooling of weld joint and coarse grain formation.
- From Response optimizer, the optimal combination for maximum fatigue life of 38,040 cycles is at Peak current 22 Amps, Back Current 12 Amps, Pulse Rate 20 pulses/sec, Pulse Width 30% which is better than experimental value of 35,787 cycles. The deviation from the predicted value is within the range of less than 6%.

Data availability All relevant data supporting the findings of this study have been included in the article and its references, as confirmed by the authors. Requests for the raw data used to support the results of this study can be made to the corresponding author.

Declarations

Conflict of interest The authors declare that they have no conflict of interests.

References

1. Nilsson, J.: Super duplex stainless steels. Mater. Sci. Technol. **8**, 685–700 (1992)
2. Nilsson, J.O., Wilson, A.: Influence of isothermal phase transformations on toughness and pitting corrosion of duplex stainless steel SAF 2507. Mater. Sci. Technol. **9**, 545–554 (1993)
3. Karlsson, L., Ryen, L., Pak, S.: Precipitation of intermetallic phases in 22% cr duplex stainless weld metals. Weld. J. **74**, 28–40 (1995)
4. Westin, E., Fellman, A.: Effect of laser and laser hybrid welding on the corrosion performance of a lean duplex stainless steel. J. Laser Appl. **22**(4), 150–158 (2010)
5. Roshan, R., Naik, A.K., Saxena, K.K., Arora, K.S., Shajan, N., Msomi, V., Mehdi, H.: Effect of welding speed and wire feed rate on arc characteristics, weld bead and microstructure in standard and pulsed gas metal arc welding. J. Adhes. Sci. Technol. **37**(23) (2023). https://doi.org/10.1080/01694243.2023.2192314
6. Nilsson, J., Kangas, P., Karlsson, T., Wilson, A.: Mechanical properties, microstructural stability and kinetics of σ phase formation in 29Cr-6Ni-2Mo-0.38 N super duplex stainless steel. Metall. Mater. Trans. A. **31**, 35–40 (2000)
7. KordatosJ, Fourlaris, G., Papadimitriou, G.: The effect of cooling rate on the mechanical and corrosion properties of SAF 2205 (UNS 31803) duplex stainless steel welds. ScriptaMetallurgica. **44**, 401–408 (2001)
8. Mcpherson, N., Samson, H., Baker, T., Fernandez, S.: Steel microstructures in autogenous laser welds. J. Laser Appl. **15**, 200–211 (2000)
9. Ku, J., Ho, N., Tjong, S.: Properties of electron beam welded SAF 2205 duplex stainless steel. J. Mater. Process. Technol. **63**, 770–775 (1997)
10. Mcpherson, N., Chi, K., Baker, T.: Submerged arc welding of stainless steel and the challenge from the laser welding process. J. Mater. Process. Technol. **134**, 174–179 (2003)
11. Omura, T., Kushida, T., Komizo, Y.: Microstructural features and corrosion properties in laser welded duplex stainless steels. Weld. Int. **14**, 257–260 (2000)
12. Capello, E., Chiarello, P., Previtali, B., Vedani, M.: Laser welding and surface treatment of a 22Cr-5Ni-3Mo duplex stainless steel. Mater. Sci. Eng., a. **351**, 334–343 (2003)
13. I.Alvarez-Armas, U., Krupp, M., Balbi, S., Herenua, M.C., Marinelli, H., Knobbe: Growth of short cracks during low and high cycle fatigue in a duplex stainless steel. Int. J. Fatigue. **41**, 95–100 (2012)
14. Roman Kolmorgen, H., Biermann: Thermo-mechanical fatigue behaviour of a duplex stainless steel. Int. J. Fatigue. **37**, 86–91 (2012)
15. Guocai Chai, R.L. Peng and, Johansson, S.: Fatigue behaviors in duplex stainless steel studied using in-situ SEM/EBSD method. Procedia Mater. Sci. **3**, 1748–1753 (2014)
16. Krupp, U., Giertler, A., Soker, M., Fub, H., Donges, B., Christ, H.J., Istomin, K., Husecken, A., Pietsch, U., Fritzen, C.-P., Ludwig, W.: Significance and mechanism of the Crack initiation process during very high cycle fatigue of Duplex Stainless Steel, XVII International Colloquium on mechanical fatigue of metals (ICMFM17). Procedia Eng. **74**, 143–146 (2014)
17. Lee, C.-H., Chang, K.-H., Van Do, V.N.: Finite element modeling of residual stress relaxation in steel butt welds under cyclic loading. Ngineering Struct. **103**, 63–71 (2015)
18. Kang, S.-W., Park, Y.-M., Jang, B.-S., Jeon, Y.-C., Kim, S.-M.: Study on fatigue experiment for transverse butt welds under 2G and 3G weld positions. Int. J. Nav Archit. Ocean. Eng. **7**, 833–847 (2015)

19. Krupp, U., Giertler, A., Soker, M., Fub, H., Donges, B., Christ, H.J., Istomin, K., Husecken, A., Pietsch, U., Fritzen, C.-P., Ludwig, W.: The behavior of short fatigue cracks during very high cycle (VHCF) fatigue of duplex stainless steel. Eng. Fract. Mech. **145**, 197–209 (2015)
20. Jinwoo Cho, C.-H., Lee: FE analysis of residual stress relaxation in a girth-welded duplex stainless-steel pipe under cyclic loading. Int. J. Fatigue. **82**, 462–473 (2016)
21. Cortes-Cervantes, I.S., Lpez-Morelos, V.H., Miyashita, Y., García-Hernandez, R., Ruiz-Marines, A., Garcia-Renteria, M.A.: Fatigue resistance of AL6XN super-austenitic stainless steel welded with electromagnetic interaction of low intensity during GMAW. Int. J. Adv. Manuf. Technol. **99**, 2849–2862 (2018)
22. Timo Bjork, H., Mettanen, A., Ahola, M., Lindgren, J., Terva: Fatigue strength assessment of duplex and super-duplex stainless steels by 4R method. Weld. World. **62**, 1285–1300 (2018)
23. Eyasin Arafat, N., Merah, F.A., Al-Badour, I.T., Bello: Jafar Albinmousa, fatigue crack growth behavior of friction stir processed super duplex stainless steels (SAF- 2507). Mater. Today Commun. **26**, 101937 (2021)
24. Sales, A.: Andrei Kotousov and Ling Yin, Design against Fatigue of Super Duplex Stainless Steel Structures Fabricated by Wire Arc Additive Manufacturing Process, Metals,11, 2021, 1965
25. Sales, A., Kotousov, A., Perilli, E., Yin, L.: Improvement of the fatigue resistance of super duplex Stainless-Steel (SDSS) Components fabricated by Wire Arc Additive Manufacturing (WAAM). Metals. **12**, 1548 (2022)
26. Janardhan, G., Kishore, K., Dutta, K., Mukhopadhyay, G.: Tensile and fatigue behavior of resistance spot-welded HSLA steel sheets: Effect of pre-strain in association with dislocation density. Mater. Sci. Engineering: A. **793**, 139796 (2020)
27. Sasidhar, Kesava Rao, V.V.S.: Investigation on effect of pulsed current micro plasma arc weld parameters on UNS S32750 super duplex stainless steel sheets. Int. J. Mod. Manuf. Technol. (IJMMT) 14 (2022)
28. Prasad, K.S., Rao, C.S., Rao, N.: Optimization of fusion zone grain size, hardness and ultimate tensile strength of pulsed current micro plasma arc welded Inconel 625 sheets using genetic algorithm. Int. J. Adv. Manuf. Technol. (Springer), Volume.85, Issue.8–12, pp.2287–2295
29. Husain Mehdi, B., Singh, A., Nait Salah, M.K., Dubey, S., Mishra, S., Kumar: Effect of PWHT on metallurgical and mechanical characterization of dissimilar welded joint of P91 and P92 steels. J. Adhes. Sci. Technol. (2023). https://doi.org/10.1080/01694243.2023.2265224
30. Sam, I., Jones, P.G., Rajakumar, S., Kavitha, S., Balasubramanian, V.: Multicriteria optimization of the weld characteristics of keyhole plasma arc welding on super austenitic stainless steel: A mathematical approach. Int. J. Interact. Des. Manuf. (IJIDeM) : 1–17. (2023)